Simultaneous Measurement of Flight Time and Energy of Large Matrix-Assisted Laser Desorption Ionization Ions with a Superconducting Tunnel Junction Detector

W. Henry Benner, David M. Horn, and Joseph M. Jaklevic
Lawrence Berkeley National Laboratory, Engineering Science Department, Human Genome Center Instrumentation Group, Berkeley, California, USA

Matthias Frank, Carl Mears, and Simon Labov
Lawrence Livermore National Laboratory, Physics and Space Technology, Livermore, California, USA

A. T. Barfknecht
Conductus, Inc., Sunnyvale, California, USA

We evaluated a cryogenically cooled superconducting Nb-Al_2O_3-Nb tunnel junction (STJ) for use as a molecular ion detector in a matrix-assisted laser desorption ionization time-of-flight (MALDI-TOF) mass spectrometer. The STJ responds to ion energy and theoretically should detect large molecular ions with a velocity-independent efficiency approaching 100%. The STJ detector produces pulses whose heights are approximately proportional to ion energy, thus the height of a pulse generated by the impact of a doubly charged ion is about twice the height of a singly charged ion pulse. Measurements were performed by bombarding the STJ with human serum albumin (HSA) (66,000 Da) and immunoglobulin (150,000 Da) ions. We demonstrate that pulse height analysis of STJ signals provides a way to distinguish with good discrimination HSA^+ from $2HSA^{2+}$, whose flight times are coincident. The rise time of STJ detector pulses allows ion flight times to be determined with a precision better than 200 ns, which is a value smaller than the flight time variation typically observed for large isobaric MALDI ions detected with conventional microchannel plate (MCP) detectors. Deflection plates in the flight tube of the mass spectrometer provided a way to aim ions alternatively at a MCP ion detector. (J Am Soc Mass Spectrom 1997, 8, 1094–1102) © 1997 American Society for Mass Spectrometry

Since the development of matrix-assisted laser desorption ionization (MALDI) by Karas and Hillenkamp [1], it has become obvious that the highest molecular masses accessible with this technique would be constrained by a decline in ion detector efficiency as ion mass is increased. This issue remains a problem today even though singly charged poly(styrene) ions as large as 1.5 MDa have been detected with microchannel plate (MCP) ion detectors [2]. Such large ions are detected inefficiently, and in practice, the upper mass limit of MALDI time-of-flight (TOF) mass spectrometers (MS) lies near a few hundred thousand Daltons when 30-keV ions are analyzed [3].

The steady decline in ion detectability that correlates with increasing ion mass is related to ion velocity. Beuhler's [4, 5] work is commonly cited in this regard because he showed the existence of a velocity threshold which must be exceeded for the yield of secondary electrons to be at least one per primary ion impact. The velocity threshold of 1×10^4 m/s is the velocity a singly charged 48,000-Da ion achieves when accelerated through 25 kV; larger singly charged ions will be detected less efficiently for the same acceleration voltage. The decline in detectability with increasing mass might be compensated by applying a higher ion acceleration voltage. The square-root dependence of ion velocity on voltage combined with high voltage engineering and safety considerations render this approach impractical. Many investigations [6] have reported the yields of secondary electrons and ions that provided insights into ways to improve ion detectability. Methods for increasing the yield of secondary electrons and ions, including the use of conversion dynodes [7], have been investigated for improving ion detection in TOF mass spectrometers. Wesmacott et al. [8] more recently reported that the efficiency for detecting ions via sec-

Address reprint requests to Dr. W. Henry Benner, Lawrence Berkeley National Laboratory, 1 Cyclotron Road, MS 70A-3363, Berkeley, CA 94720. E-mail: whbenner@lbl.gov

1044-0305/97/$17.00
PII S1044-0305(97)00147-5

Received February 28, 1997
Revised May 21, 1997
Accepted May 21, 1997

ondary electron emission declines steadily with mass yet remains above about 30% at 300,000 Da and 30-kV acceleration. They also reported that detection schemes based on secondary negative ion formation are more efficient and remain near 100% efficiency for 30-keV ions <300,000 Da. However, time resolution is compromised in secondary negative ion detection schemes, which makes this approach less attractive. While many studies regarding secondary electron or ion formation were conducted by bombarding metal or aluminum oxide surfaces with primary ions, the relationship of these results to the yield of secondary electrons or ions generated on the surface or in the channels of a MCP detector by the impact of large ions is not clear. The response of MCP detectors to large ion impacts remains poorly characterized.

Recently we showed that the poor detection efficiency exhibited by MCPs for large ions might be solved by cryogenic detector technology [9]. Cryogenic detectors comprise a new class of particle and x-ray detectors that do not rely on ionization but register the impact of individual particles, charged or not, by responding to the deposited energy. A fundamental description of the various types of cryogenic detectors is not within the scope of this paper but their description can be found in the literature [10, 11]. Already in 1991 as a component to a detector development project [12], we considered using bolometric detectors [13] as an ion detector in a TOF mass spectrometer. However, the detectors available at that time were mostly bolometers with a time response too slow for timing applications encountered in MALDI-TOF-MS. More recently, Twerenbold [14] suggested the use of other versions of cryogenic detectors, such as superconducting tunnel junction (STJ) devices, which are much faster and more applicable.

In a STJ detector, two superconducting films are separated by a thin insulator. When a particle, such as a MALDI ion, strikes one of the films, the kinetic energy of the ion creates nonthermal phonons in the films, which in turn cause Cooper pairs (weakly associated electrons) to break apart. Quasiparticles (electronlike or holelike excitations in the superconductor) are created and quantum-mechanically tunnel through the thin insulator, producing a current pulse when a small bias voltage in the order of 1 mV is applied to the junction. Only a few millielectron volts are required to break a Cooper pair and therefore the kinetic energy of a 25-keV ion produces many quasiparticles, about 2 million for the detector used in this study. The magnitude of the tunneling current pulse is proportional to the number of quasiparticles produced, which in turn corresponds roughly to the amount of energy deposited into the detector by an impacting ion. Twerenbold et al. [15] recently described the operation of a MALDI-TOF-MS using a Sn-SnO_x-Sn STJ detector. The detector was operated at 0.3 K, which necessitated the use of a ^{3}He cryostat. They generated a mass spectrum of 20-keV ions with this detector, demonstrating for the first time the application of a cryogenic detector as an ion detector in a MALDI-TOF-MS. They observed that 10-keV ions of lysozyme produced detector pulses about equal in magnitude to the pulses generated with 6-keV x rays but did not report the discrimination of multiply charged ions via ion energy measurements. In a series of similar experiments we tested one of our Nb-AlO_x-Nb STJ detectors in our MALDI-TOF-MS and described the detection [9] of 66,000-Da human serum albumin (HSA) ions with the STJ detector. Here, we discuss additional data concerning mostly the energy resolving capability of our STJ detectors. Our STJ detector can be used to discriminate different charge states of the ions even though the energy resolution for MALDI ions appears to be less than that observed for x rays. The ability to determine ion energy may be particularly valuable for resolving ambiguities when samples with several ion species and several charge states are studied.

Experimental

Our experimental setup was described previously in more detail [9] and therefore only the salient features are summarized here. Our STJ detector consists of a 100-nm-thick top niobium film separated by a 2-nm aluminum oxide tunneling barrier from a lower 260-nm-thick niobium film on a silicon substrate. The active area of the detector is 0.04 mm^2. Niobium becomes superconducting at 9.2 K but to minimize the thermal breaking of Cooper pairs we typically operate the detector at 1.3 K. This temperature is achieved by mounting the detector at the end of the flight tube in a pumped ^{4}He cryostat, which is evacuated by the mass spectrometer's vacuum system. The cryostat used in this study is approximately 19 cm diameter and 40 cm tall and does not take up significant additional space when it is attached to our MALDI-TOF-MS. The resulting current pulses produced by x rays and macromolecular ions striking the STJ are measured with a field effect transistor (FET) based amplifier operating at room temperature. The impact of 25-keV ions results in pulses with pulse heights around 100–200 mV. The output of the amplifier was digitized and saved for offline processing.

The MALDI-TOF mass spectrometer used in this study was described previously [16]. It was modified for this study so that our STJ and MCP detectors could be operated simultaneously. The STJ detector was aligned with the centerline of the flight tube, which necessitated mounting the 2.5-cm-diameter MCP detector off center. Deflection plates located in the flight tube provided a way to deflect ions toward the MCP detector. This setup provides a way to collect spectra with both detectors, but because the deflection plates will only deflect ions, the response registered by the MCP detector will not include signals produced by high velocity neutral molecules or fragments. Neutrals travelling fast enough to produce a signal on either detector will originate by metastable decay of ions as they traverse the flight tube. The extent of metastable decay

is related to ion internal energy, and this varies with launching conditions and the composition of the matrix. Large molecular ions have been reported to experience metastable decay more readily than small ions [17]. Therefore, it is likely that the centered STJ detector will be bombarded by neutrals while the MCP will not. The mass spectrometer includes two features not typical of most MALDI-TOF-MS. First, the sample is applied to a probe that is continually rotated so that fresh areas of the sample are brought into the spot where the laser hits the target. This feature is particularly useful in helping to maintain a stabilized ion flux while collecting data with each detector. Second, we apply the sample onto the vacuum side of a window in the end of the sample probe and illuminate the sample from the backside by shining the laser beam through the window. This rear illumination technique is not necessary for conducting the tests we describe here but allowed ion-focusing elements to be operated in other ongoing experiments. The samples were illuminated at about 3 Hz with approximately 3-ns-wide light pulses (335 nm) from a N_2 laser. The laser intensity was adjusted with a variable neutral density filter to a level that slightly exceeded the threshold required for producing analyte ions. The dual MCP assembly was biased at −1800 V in this test (−1900 V on the MCP surface that receives ions and −100 V on the output side of the second MCP).

Samples comprising 1 μL of 10^{-4} M human serum albumin (HSA) or anti-DNA immunoglobulin G (IgG) in water plus 1-μL saturated sinapinic acid in 1:1 acetonitrile: water were applied to the quartz window and evaporated under flowing N_2. The concentrations employed are relatively high and were chosen to increase ion production and also to increase the production of multiply charged ions. The liquid sample was rubbed with the tip of a plastic micropipette tip as it dried so that small crystals resulted. HSA and sinapinic acid were purchased from Sigma Chemical Co. The IgG immunoglobulin was purchased from Biodesign (Kennebunk, ME).

Results

Figure 1 shows a single-shot TOF record acquired with the STJ detector from a sample containing HSA (66,000 Da). The pulses rising above the baseline are due to the impact of ions. Individual ion impacts generate STJ detector pulses having a rise time of 500 ns and a decay time of about 1.5 μs. Pulses derived from individual ions are identified by their height and width. In this figure, many of the pulses occurring after about 40 μs are attributable to individual ions. Pulse pileup is obvious at shorter flight times due to the large number of hits by matrix ions. Our pulse analysis procedure, described below, provides a way to distinguish most pileup events from single ion events.

Even though the STJ detector has an active area of only 0.04 mm^2, many ions strike the detector every time the laser is fired. The number of pulses shown in Figure 1 is typical of a single-shot record but the occurrence of

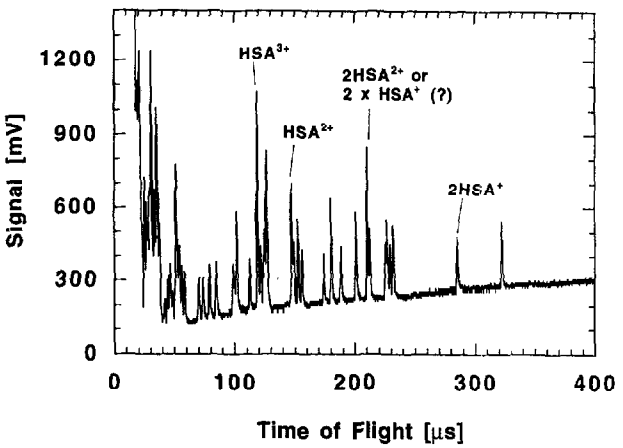

Figure 1. A single-shot TOF record acquired with the STJ detector from a sample of HSA (66,000 Da) in sinapinic acid. Pulses which rise less than about 250 mV above the background are likely singly charged matrix ions. Ion energy was 25 keV/charge.

the three types of monomeric ions (as labeled) in a single laser shot is exceptional. This record was chosen to show that ions with higher charge, and therefore higher energy, produce larger pulses when they strike an energy-responding STJ detector. Most of the individual pulses in Figure 1 are presumably caused by aggregated matrix ions. Pulses corresponding to the expected flight time for HSA^{3+}, HSA^{2+}, HSA^{+}, or $2HSA^{2+}$ and $2HSA^{+}$ are indicated in this figure. Mass assignments are based on flight times. It is not certain that the indicated individual pulses were actually caused by HSA ions. It is possible that the indicated pulses were due to agglomerated matrix ions having flight times the same as expected for HSA ions. However, when single-shot spectra are summed and averaged, peaks corresponding to HSA^{+}, HSA^{2+}, and HSA^{3+} become apparent. Also, pulse height analysis, discussed below, corroborates our assignment of charge to the pulses. The pulse heights of the 3+ ion and the 2+ ion, respectively, are about three times and two times as large as pulses assigned to the $2HSA^{+}$ ion or the numerous singly charged matrix ions. Implications derived from pulse height analysis of the detector pulses will be discussed in more detail later in this article.

In addition to pulses generated by single ion impacts, the spectrum in Figure 1 displays several other distinctive features. A large positive transient occurs during the first several microseconds of the flight time record. It is caused by a large number of matrix ions hitting the detector along with laser light striking the detector. The large number of matrix ions and the laser light pulse momentarily warm the superconducting films in the detector, creating a large tunneling current. During this transient, the detector is insensitive to individual ion impacts. A rising baseline follows this transient because the FET amplifier is momentarily

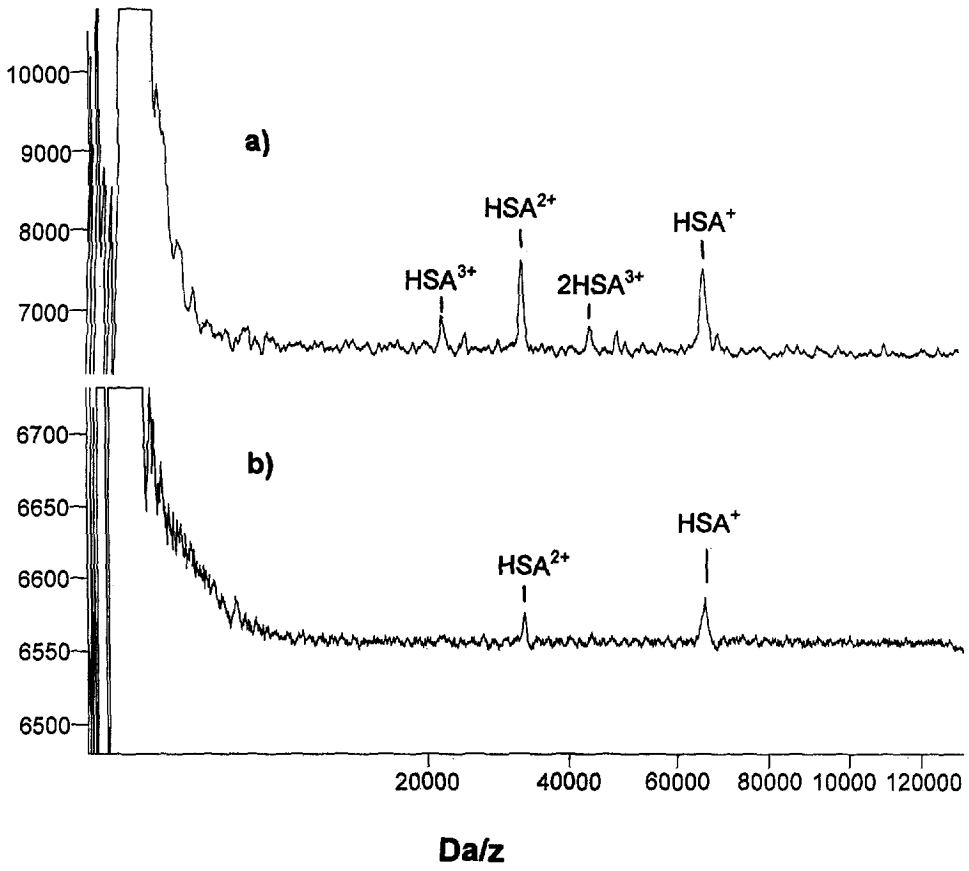

Figure 2. (a) The mass spectrum of HSA produced by summing and averaging 46 single-shot STJ spectra. The acceleration voltage was 25 kV (ion energy = 25 keV/charge) and the vertical axis is relative intensity. Mass assignments are made from flight times and pulse height information. (b) A mass spectrum of HSA acquired with a MCP detector using the same sample as shown in a. 355 single laser shots were summed and averaged and the data (1-GHz sampling rate) was then smoothed with a 50-pt running average. The acceleration voltage was 25 kV (ion energy = 25 keV/charge) and the vertical axis is relative intensity.

overwhelmed by the large tunneling current produced and requires several hundred microseconds to recover completely. The thermal coupling between the detector and the cryostat is robust enough so that the detector cools back down to operating temperature in less than 20 μs. The initial overshoot and the recovering baseline do not impose a problem for time-of-flight measurements and could be avoided, if desired, by aiming the laser slightly away from the STJ detector and deflecting the matrix ions.

When single-shot STJ TOF records from a HSA sample are summed and averaged, as is commonly done to create TOF spectra with MCP detectors, the mass spectrum in Figure 2a is produced. The four major peaks in this spectrum can be assigned to HSA^+, HSA^{2+}, $2HSA^{3+}$, and HSA^{3+} simply by their times of flight. The detection of these four types of HSA ions is remarkable in light of the fact that only 46 single-shot STJ spectra were averaged. Peaks from several additional minor components are also seen in this spectrum but their mass assignment is speculative. For example, the small peak near 50,000 could possibly be assigned to $3HSA^{4+}$, which has a calculated Da/z of 49,500. When the energy-resolving capability of the STJ detector is considered later in this paper, additional types of HSA ions are detectable.

An averaged MCP detector spectrum was also obtained for HSA, shown in Figure 2b, by deflecting the ions from 355 shots towards the MCP detector. It was generated from the same sample that was used to generate the mass spectrum in Figure 2a. The data used to generate this spectrum was smoothed with a 50-pt. running average. Without the smoothing process, the ion peaks were barely discernible. Two peaks can be identified in this average spectrum that correspond to HSA^+ and HSA^{2+}. One caveat should be emphasized before Figure 2a and b are compared. Individual STJ pulses are much wider than MCP pulses. The wider STJ pulses accumulate more readily on top of each other than do the narrow pulses from a MCP when spectra

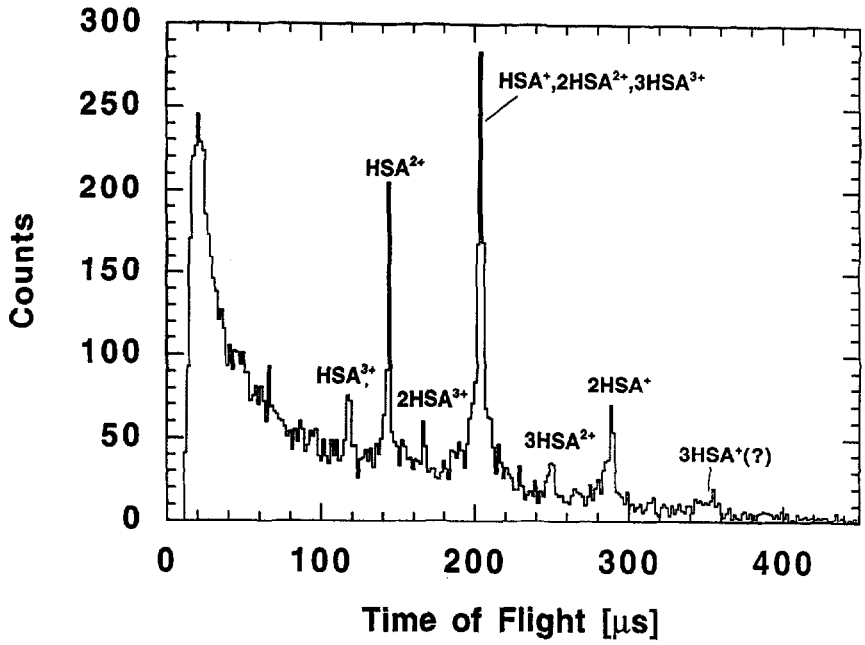

Figure 3. A mass spectrum generated from HSA in sinapinic acid using the STJ detector. Individual detector pulses from 500 STJ single-shot spectra were digitally filtered, as described in the text, to determine more accurately individual ion arrival time. "Counts" refers to the number of pulses occurring in 1.7-μs-wide time bins. Ion energy was 25 keV/charge.

from each detector are summed and averaged, making the peaks in the averaged STJ mass spectrum appear large in comparison.

In order to enhance the timing resolution of the STJ detector and extract pulse heights, TOF records from individual laser shots are digitally processed in the following way. TOF records from the STJ are first smoothed with a digital 500-kHz low-pass filter and then differentiated. The start time of each pulse is then taken as the time that the derivative slightly exceeds the noise level of the amplifier. If pulses occurred between about 200 ns and 1 μs of each other, only the first pulse is processed. If pulses occurred within 200 ns of each other, they are treated as a single pulse. This pileup cut rejects about 25% of the detector pulses and misses only a small number of real pileup events. When single-shot STJ spectra are processed in this manner, ion arrival time can be determined to better than 200 ns. We note that while this data analysis procedure was done in digital form offline after the data was recorded, equivalent data processing could be performed on-line with analog electronics. Figure 3 shows a TOF spectrum obtained by processing 500 single-shot STJ records. Several singly, doubly, and triply charged albumin peaks can easily be identified. Assignment of HSA^+, $2HSA^{2+}$, and possibly $3HSA^{3+}$ to the peak at 210 μs is based on flight time and detector pulse height.

The energy-dependent response of the STJ detector provides a way to discriminate ions of different charge. Doubly charged ions, for example, carry twice the kinetic energy of singly charged ions and generate pulses with about twice the height. In Figure 4 we show a scatter plot of pulse height versus flight time (for the same data as used for Figure 3). Every point in this plot corresponds to a detector pulse. The "dark band" of events with pulse heights smaller than about 250 mV can be assigned to singly charged ions. This can be seen when a pulse height cut is made at 250 mV along the horizontal line in this figure. The TOF spectrum for a

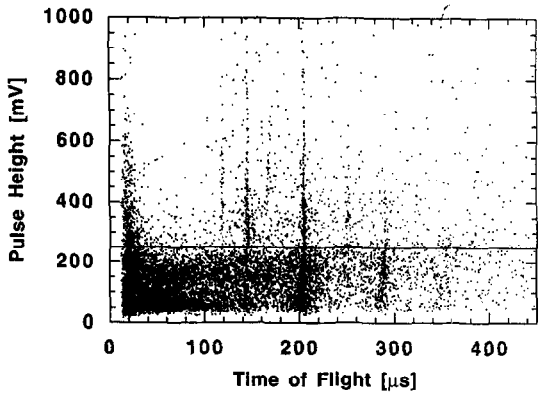

Figure 4. A plot of STJ detector pulse height as a function of ion flight time. The data used to prepare this plot are the same as used in Figure 3 and are presented to show the utility of an energy responding ion detector. The horizontal line at 250 mV describes the pulse height cut used to segregate multiply charged ions from singly charged ions.

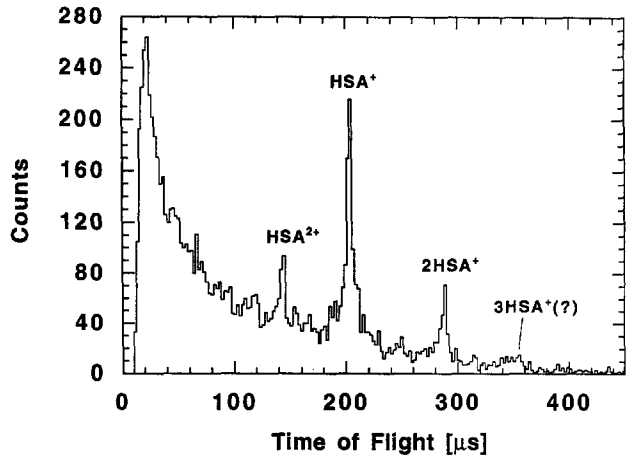

Figure 5. The mass spectrum of a HSA sample that results when a pulse height cut is made to exclude STJ pulses larger than 250 mV from the data presented in Figure 4. "Counts" refers to the number of pulses accumulated in 2.2-μs-wide time bins.

collection of ions with pulse heights <250 mV (Figure 5) shows peaks that are assigned mostly to singly charged ions. This cut enhances the visibility of singly charged ions in the TOF spectrum. Peaks assigned to multiply charged ions are removed or at least strongly suppressed in Figure 5 by removing pulses larger than 250 mV. The distribution of the mass of the matrix ions appears as a broad peak at relatively short flight times. In contrast, the TOF spectrum of events with pulse height >250 mV (Figure 6) contains mostly multiply charged ions. The broad peak between 20 and 40 μs in Figure 6 is likely attributable to pulses resulting when more than one matrix ion strikes the detector simultaneously, thereby creating pulses larger than expected for singly charged ions.

The pulse height cut at 250 mV (Figure 4) does not discriminate perfectly singly charged ions from multiply charged ones, as evidenced by the presence of the HSA^{2+} ion peak in Figure 5 and $2HSA^{+}$ in Figure 6. Imperfect discrimination occurs for two reasons. First, this STJ detector shows a poorer energy resolution for macromolecular ions than for x rays. The energy resolution of this STJ detector is only about 20 keV [based on the full width at half maximum (FWHM) of the pulse height distribution] for macromolecules and therefore pulse height distributions from singly and doubly charged ions, with 25- and 50-keV energy, respectively, overlap and cannot be perfectly separated. This rather poor energy resolution for macromolecules is in contrast to the observed FWHM energy resolution of 300 eV for 6-keV x rays. 6-keV x rays deposit their energy directly in the Nb films of the STJ detector, thus generating quasiparticles relatively efficiently. Macromolecules deposit their energy on the surface of the STJ, producing phonons. Only a fraction of these phonons is subsequently absorbed by the Nb film, thus creating a smaller signal. From the measured pulse heights, we infer that 6-keV x rays produce about 2.5 million quasiparticles and 25-keV macromolecular ions produce about 2 million quasiparticles. The relatively smaller signal produced by macromolecular ions cannot be the only reason for the poor energy resolution observed for ions. We do not yet understand in detail

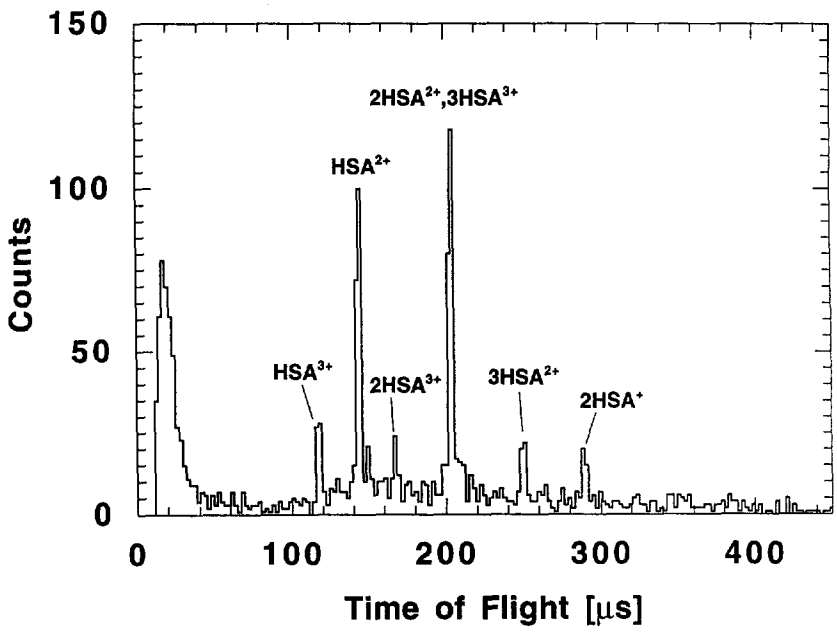

Figure 6. The mass spectrum of a human serum albumin sample that results when a pulse height cut is made to exclude STJ pulses less than or equal to 250 mV from the data shown in Figure 4. "Counts" refers to the number of pulses accumulated in 2.2-μs-wide time bins.

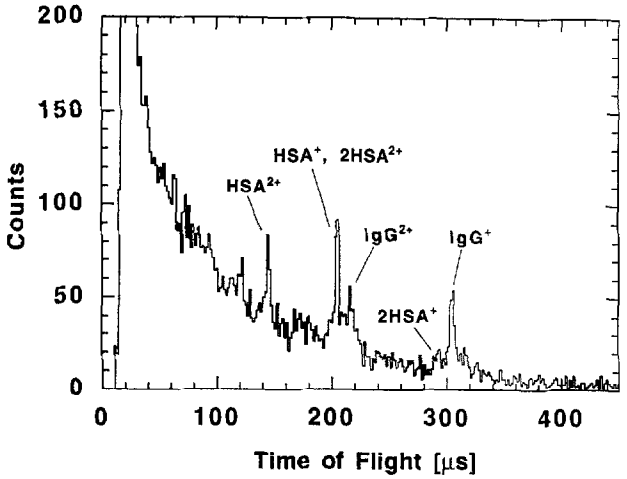

Figure 7. A STJ mass spectrum generated from a sample of HSA and an IgG immunoglobulin in sinapinic acid. This histogram contains pulses from 500 laser shots. Ion energy was 25 keV/charge. "Counts" refers to the number of pulses accumulated in 1.7-μs-wide bins.

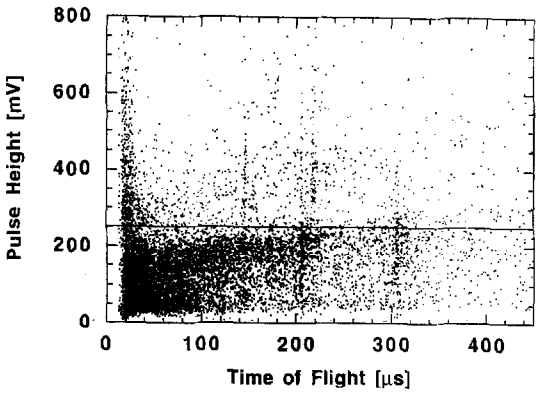

Figure 8. A plot of STJ detector pulse height as a function of ion flight time for the same data used in Figure 7. The horizontal line at 250 mV describes the pulse height cut used to segregate multiply charged ions from singly charged ions.

the way in which a macromolecular ion transfers its energy to the Nb films. Another reason for poor energy resolution could be ion fragmentation. If an ion fragments after impact, releasing smaller fragments that fly away from the detector, the energy transfer process could be inefficient and variable.

The second reason for poor discrimination of ion charge could result from the way the pulse height cut is made. The top of the dark band comprising singly charged pulses (Figure 4) is not flat and perhaps the height of the cut should increase with flight time. We do not yet know why the pulse height for singly charged ions become larger at longer flight times. This imperfect pulse height cut could explain the persistence of the $2HSA^+$ peak at 287 μs in Figure 6 because the cluster of points at 287 μs in Figure 4 rises a little above the line.

An estimate of the relative contribution of each component to the peak at 204 μs in Figure 3 indicates that HSA^+ comprises approximately 75% of the counts. This peak, assigned to HSA^+, $2HSA^{2+}$, and possibly $3HSA^{3+}$, contains 1123 counts in 11 bins stretching between 194.5 and 213.1 μs. About 330 of these counts can be assigned to background matrix ions by interpolating the number of ions appearing in bins adjacent to the peak. This leaves 793 counts attributable to HSA ions. The comparable peak in Figure 5 contains 834 counts in eight time bins between 193.6 and 212.0 μs, of which about 240 are background matrix ions, and thus 594 are HSA^+ ions. The existence of $3HSA^{3+}$ is plausible in light of the observed existence of HSA^{3+} and $2HSA^{3+}$. Not enough triply charged ion pulses were sampled for a reliable estimate of their pulse height to be determined and used to calculate their fractional contribution to the peak at 204 μs. There are a few pulses in this peak that are more than three times larger than 250 mV that might be assigned to $3HSA^{3+}$. Thus, the remaining 25% of the counts in the peak at 204 μs is an upper estimate for the contribution by $2HSA^{2+}$ ions. Without an energy-resolving detector, the peak at 204 μs would have simply been assigned to HSA^+.

Next we present STJ data derived from a mixture containing HSA and an IgG (150,000 Da). This sample was used to evaluate the capability for identifying components in mixed samples and to examine the response of the detector with impacts produced with much higher mass ions. The data used to compile the STJ spectrum in Figure 7 were processed by the digital analysis technique described above. The spectrum contains peaks that can be assigned to the single and doubly charged ions of HSA and IgG, thus demonstrating the capability for identifying the components of this two-component mixture. Corroboration of the mass assignments presented in Figure 7 is facilitated by examining a plot of STJ pulse height versus flight time, as shown in Figure 8. Clusters of points can be seen in this plot which help to assign charge states to the peaks in the mass spectrum in Figure 7. The band of data points corresponding to pulse heights below about 250 mV are assigned to ions carrying a single charge and multiply charged ion pulses lie above this band. In the distribution of points that occurs just after 200 μs in Figure 8, it can be seen that a cluster appears in the background noise that has a peak height corresponding to ions with one charge. This cluster lies below the 250-mV line. Slightly later in this record is another cluster of pulses with heights greater than about 250 mV. When a pulse height cut of 250 mV, as indicated by the horizontal line in Figure 8, is used to discriminate against doubly charged ions, the spectrum in Figure 9 is obtained. The two largest peaks in this plot are assigned

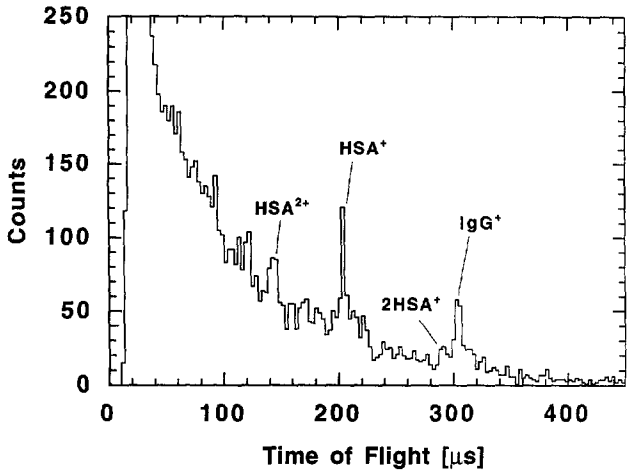

Figure 9. The mass spectrum of a sample containing HSA and immunoglobulin that results when a pulse height cut is made to exclude STJ pulses larger than 250 mV from the data shown in Figure 8. Most of the background events are due to the mass distribution of singly charged matrix ions. "Counts" refers to the number of pulses accumulated in 2.8-μs-wide time bins.

to singly charged ions but a small peak assigned to HSA^{2+} remains. This results because the energy resolution of this STJ detector is about 20 keV and the overlap in the pulse height distributions for singly and doubly charged ions, discussed above, does not permit perfect discrimination between 25- and 50-keV ions. Figure 10 shows the peaks that result when pulses larger than 250 mV are selected from the data used in Figure 8. This cut eliminates nearly all singly charged ions from the spectrum. The peak between 20 and 50 μs is due possibly to more than one matrix ion striking the detector simultaneously, thus creating pulses larger than expected for singly charged ions. The pulse height cut revealed an additional ion in the spectrum, namely the triply charged IgG ion, which was buried in the data plotted in Figure 8. The peak due to the triply charged IgG molecular ion would not have been detected without the application of the pulse height analysis procedure. The plots in Figures 9 and 10 of energy-segregated pulses clearly demonstrate that an energy-resolving STJ detector helps to facilitate peak assignments.

Finally, a MCP detector was used to collect a mass spectrum from the same sample of HSA and IgG analyzed in Figures 7–10. The MCP spectrum is shown in Figure 11. The quality of this spectrum is notably poorer than the spectrum generated with the STJ detector. In particular, the IgG peaks are broader than those generated by the STJ detector. This is perhaps attributable to the deflection of the ions towards MCP mounted off axis. The deflection could have distorted the beam and broadened the timing spread of the ions. Future experiments will be conducted to compare the response of the two detector types. We plan to repeat these experiments using a MCP detector with an annular aperture and a STJ detector mounted behind the aperture. The use of an annular MCP detector avoids possible beam distortions that might be caused by deflecting the ion beam and will provide us with an improved way for comparing the sensitivity of the two detectors.

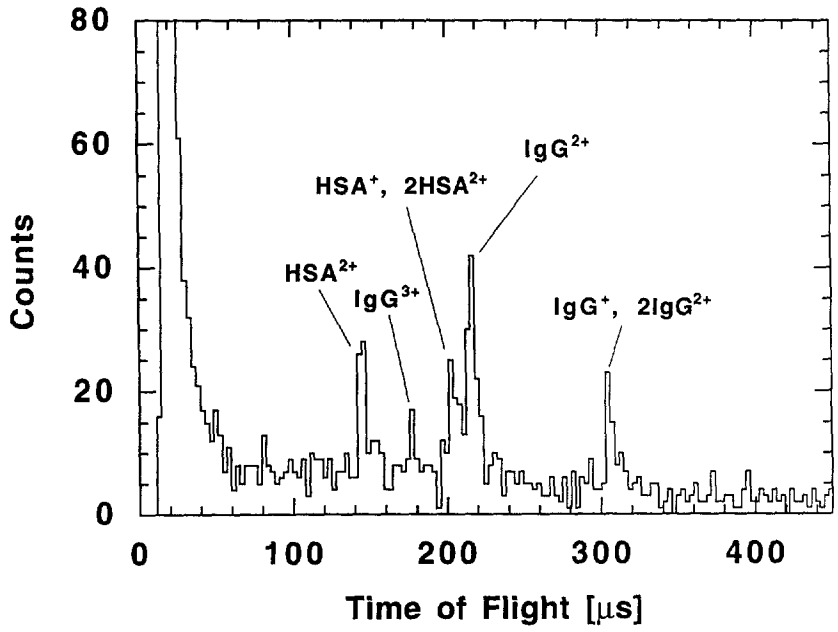

Figure 10. The mass spectrum of a sample containing HSA and immunoglobulin that results when a pulse height cut is made to exclude STJ pulses less than or equal to 250 mV from the data shown in Figure 8. "Counts" refers to the number of pulses accumulated in 2.8-μs-wide time bins.

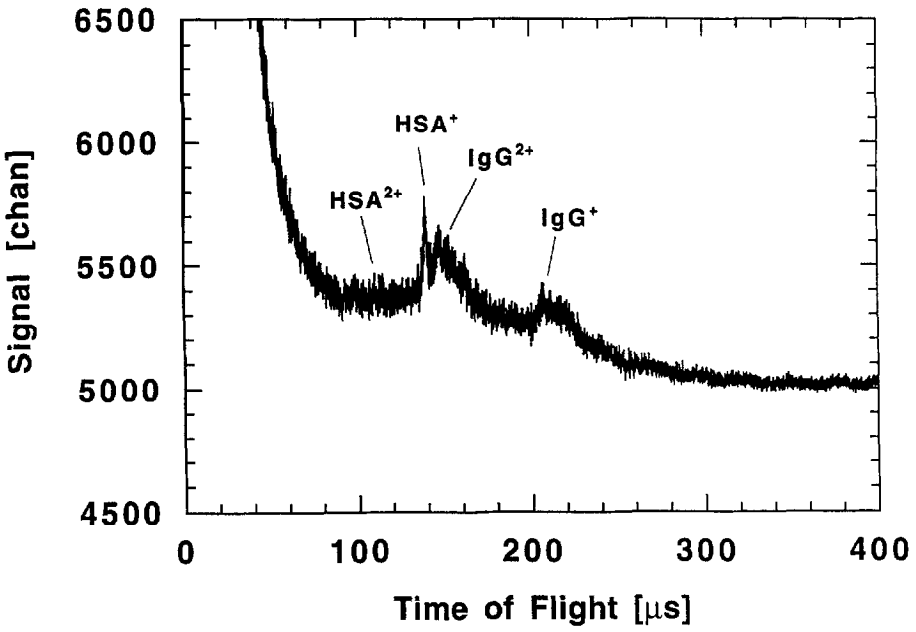

Figure 11. A mass spectrum generated with a MCP ion detector from the same sample used to produce data in Figure 8. Flight times in this figure are different from those in previous figures because the flight path to the MCP detector was 122 cm, but 173 cm to the STJ detector. One hundred shots were averaged and the ion energy was 25 keV/charge.

Conclusions

Our work shows that cryogenic detectors, such as superconducting tunnel junctions operating at 1.3 K, can easily be used for detecting ions in MALDI-TOF-MS. We show that our STJ detector is energy sensitive and can be used to detect 150,000-Da ions. This detector technology provides a way to detect very large molecular ions in TOF mass spectrometers and ions larger than 150,000 Da should be detected with this technology. The energy response capability of the detector introduces a way to detect, for example, isochronic ions of different charge.

Acknowledgments

The authors would like to thank Damian Twerenbold for stimulating discussions and Jan Batteux and William Searles for their expert technical support. This work was supported by the Director, Office of Energy Research, Office of Health and Environmental Research, Human Genome Program, of the U.S. Department of Energy under Contract No. DE-AC03-76SF00098. This work was also performed under the auspices of the U.S. Department of Energy by Lawrence Livermore National Laboratory under Contract No. W-7405-ENG-48.

References

1. Karas, M.; Hillenkamp, F. *Anal. Chem.* **1988,** *60,* 2299–2301
2. Schriemer, D. C.; Li, L. *Anal. Chem.* **1996,** *68,* 2721–2725
3. Hillenkamp, F.; Karas, M.; Beavis, R. C.; Chait, B. T. *Anal. Chem.* **1991,** *63,* A1193–A1202
4. Martens, J.; Ens, W.; Standing, K. G.; Verentchikov, A. *Rapid Commun. Mass Spectrom.* **1992,** *6,* 147–157, and references therein
5. Kaufmann, R.; Kirsch, D.; Rood, H. A.; Spengler, B. *Rapid Commun. Mass Spectrom.* **1992,** *6,* 98–104
6. Buehler, R. J.; Friedman, L. *Nucl. Instrum. Methods B* **1980,** *170,* 309–315
7. Xu, Y.; Bae, Y. K.; Buehler, R. J.; Friedman, L. *J. Phys. Chem.* **1993,** *97,* 11883–11886
8. Westmacott, G.; W. Ens; Standing, K. G. *Nucl. Instrum. Methods B* **1996,** *108,* 282–289
9. Frank, M.; Mears, C.; Labov, S.; Benner, W. H.; Horn, D. M.; Jaklevic, J. M. *Rapid Commun. Mass Spectrom.* **1996,** *10,* 1946–1950
10. Twerenbold, D. *Rep. Prog. Phys.* **1996,** *59,* 349–426
11. Booth, N. E.; Goldie, D. J. *Supercond. Sci. Technol.* **1996,** *9,* 493–516
12. Jaklevic, J. M.; Benner, W. H.; Katz, J. "Advanced Detectors for Mass Spectrometry," unpublished.
13. Sadoulet, B. *IEEE Trans. Nucl. Sci.* **1988,** *35,* 47–54
14. Twerenbold, D. *Nucl. Instrum. Methods B* **1996,** *370,* 253–255
15. Twerenbold, D.; Vuilleumier, J.-L.; Gerber, D.; Tadsen, A.; Brandt, B. van d.; Gillevet, P. M. *Appl. Phys. Lett.* **1996,** *68,* 3503–3505
16. Benner, W. H.; Horn, D. M.; Katz, J.; Jaklevic, J. M. *Rapid Commun. Mass Spectrom* **1995,** *9,* 537–540
17. Karas, M.; Bahr, U.; Strupat, K.; Hillencamp, A. *Anal. Chem.* **1995,** *67,* 675–679